Acta Crystallographica Section D
Biological Crystallography
ISSN 0907-4449

Role of the MotB linker in the assembly and activation of the bacterial flagellar motor

Jenna O'Neill,[a] Meng Xie,[a] Marcel Hijnen[b] and Anna Roujeinikova[b,c]*

[a]Manchester Interdisciplinary Biocentre, University of Manchester, 131 Princess Street, Manchester M1 7DN, England, [b]Department of Biochemistry and Molecular Biology, Monash University, Clayton, Victoria 3800, Australia, and [c]Department of Microbiology, Monash University, Clayton, Victoria 3800, Australia

Correspondence e-mail: anna.roujeinikova@monash.edu

Received 27 August 2011
Accepted 5 October 2011

PDB References: MotB variants, 3s0y; 3s02; 3s03; 3s06; 3s0h; 3s0w.

Bacterial flagella are driven by an ion influx through the peptidoglycan (PG)-tethered MotA/MotB stator. Stator precomplexes assemble in the membrane and remain inactive until they incorporate into the motor, upon which MotA/MotB changes conformation. The nature of this change and the mechanism of inhibition of the PG-binding and ion-conducting activities of the precomplexes are unknown. Here, the structural analysis of a series of N-terminally truncated MotB fragments is presented, the mechanism of inhibition by the linker is identified and the structural basis for the formation of the PG-binding-competent open-channel MotA/MotB conformation *via* a mechanism that entails linker unfolding and rotational displacement of MotB transmembrane helices is uncovered.

1. Introduction

The stator ring of the proton-motive-force-driven bacterial flagellar motor is composed of several anchored $MotA_4MotB_2$ complexes, the proton influx through which generates a turning force (torque) acting on the rotor (reviewed in Terashima *et al.*, 2008). MotA engages the rotor *via* electrostatic interactions with FliG. The C-terminal domain of MotB (MotB-C) tethers the stator complex to peptidoglycan (PG) of the cell wall around the rotor (Roujeinikova, 2008; Reboul *et al.*, 2011). MotB dimerization *via* MotB-C is essential for its function (Kojima *et al.*, 2009; Roujeinikova, 2008). Previous analysis of the structure of (*N*-acetylmuramic acid)-bound MotB-C from *Helicobacter pylori* (*Hp*MotB-C_{125}; residues 125–256) suggested that two sugar chains of PG can bind simultaneously to the two halves of the MotB dimer (Roujeinikova, 2008). The N-terminal transmembrane (TM) single-α-helix segments of the two MotB molecules in the stator complex are proximal to each other and are surrounded by the TM helices of four MotA molecules. The TM helix of MotB and helices TM3 and TM4 of MotA constitute a proton channel, which is likely to have a configuration with two channels per $MotA_4MotB_2$ complex.

Previous studies of MotB-C from *H. pylori* (*Hp*MotB-C_{125}; Roujeinikova, 2008) and *Salmonella typhimurium* (*St*MotB-C_{99}; residues 99–276; Kojima *et al.*, 2009) revealed that they share a strongly conserved 100-residue structural core with outer membrane protein A-like PG-binding proteins, including PG-associated lipoprotein (Pal). *Escherichia coli* MotB-C can be replaced by the PG-binding domain of *E. coli* Pal without loss of function (Hizukuri *et al.*, 2009), indicating that the major role of this domain is PG association.

$MotA_4MotB_2$ complexes are believed to assemble in the membrane and to remain inactive until they incorporate into the motor (Wilson & Macnab, 1988; Hosking *et al.*, 2006),

Table 1
X-ray data-collection and phasing statistics.

Values in parentheses are for the highest resolution shell.

	MotB-C_{64}	MotB-C_{78}	MotB-C_{90}	MotB-C_{97}, low-pH form	MotB-C_{97}, high-pH form	MotB-C_{103}
Space group	$P4_32_12$	$P4_32_12$	$P4_3$	$P3_121$	$P4_3$	$P3_121$
Unit-cell parameters						
a (Å)	75.2	74.7	73.0	70.7	71.7	75.8
b (Å)	75.2	74.7	73.0	70.7	71.7	75.8
c (Å)	124.7	126.5	127.2	143.4	126.2	140.8
β (°)	90	90	90	120	90	120
Resolution range (Å)	20–1.8 (1.90–1.80)	30–2.5 (2.64–2.50)	30–2.1 (2.21–2.10)	30–1.8 (1.90–1.80)	30–2.5 (2.64–2.50)	30–2.5 (2.64–2.50)
Completeness (%)	91 (91)	99 (99)	98 (99)	98 (99)	85 (88)	99 (99)
Observed reflections	162389	71074	97787	214679	65271	88035
Unique reflections	30716	12864	37792	38287	18607	16795
Average $I/\sigma(I)$	16.8 (3.5)	17.9 (5.0)	6.8 (2.5)	16.0 (4.2)	7.6 (2.7)	14.5 (4.9)
$R_{\rm merge}$† (%)	0.062 (0.331)	0.067 (0.333)	0.098 (0.343)	0.066 (0.329)	0.109 (0.319)	0.090 (0.275)

† $R_{\rm merge} = \sum_{hkl}\sum_i |I_i(hkl) - \langle I(hkl)\rangle| / \sum_{hkl}\sum_i I_i(hkl)$, where $I_i(hkl)$ is the intensity of the ith observation of reflection hkl.

whereupon the linker connecting the TM helix and the PG-binding domain of MotB is thought to extend, possibly *via* unfolding (Kojima *et al.*, 2009). Leake *et al.* (2006) observed rapid turnover of GFP-MotB between the membrane pool and the motor and estimated that a new stator complex associates with the motor every ∼0.5 min. MotB-containing precomplexes diffusing in the membrane do not bind significantly to the cell wall (Leake *et al.*, 2006), which is in line with the observation by Kojima *et al.* (2008) that MotB (in the membrane pool) could not be co-isolated with PG under conditions where Pal works as a positive control. Little is known about the mechanism of stator association and activation. We propose that the linker region of MotB stabilizes the MotB dimer in a form that is not competent for binding to PG. To support this hypothesis, we present the crystallographic analysis of a series of N-terminally truncated *Hp*MotB variants comprising the PG-binding domain and part of the linker. This analysis reveals how the structure responds to linker separation and suggests a mechanism of MotB activation that entails linker unfolding and rotational displacement of MotB transmembrane helices.

2. Experimental

2.1. Crystallography

Recombinant *Hp*MotB was produced as described previously (O'Neill & Roujeinikova, 2008). MotB-C_{78} (residues 78–256), MotB-C_{90} (residues 90–256) and MotB-C_{97} (residues 97–256) were purified following a similar procedure. Crystals were grown by the hanging-drop vapour-diffusion method at 293 K using protein concentrations of 8–16 mg ml^{-1}. MotB-C_{64} (residues 64–256) and MotB-C_{103} (residues 103–256) crystals were obtained as a result of proteolytic degradation of *Hp*MotB during the crystallization process. The reservoir solution for MotB-C_{64} has been described previously (O'Neill & Roujeinikova, 2008). The reservoir solution for MotB-C_{103} consisted of 100 m*M* MES pH 6.5, 6% PEG 20K. Crystals of MotB-C_{78} were obtained using 100 m*M* Tris pH 8.5, 2.5 *M* ammonium sulfate (AS) as a reservoir solution. Crystals of MotB-C_{90} were grown using a reservoir solution consisting of 100 m*M* HEPES pH 7.5, 2% PEG 400, 2 *M* AS. Low-pH and high-pH forms of MotB-C_{97} were obtained using reservoir solutions consisting of 100 m*M* citric acid pH 5.0, 0.8 *M* AS and of 100 m*M* Bicine pH 9.0, 2 *M* AS, respectively. Diffraction data were collected at 100 K using the Swiss Light Source (PX06, Villigen, Switzerland) and ESRF beamline ID14-4, and were processed using *MOSFLM* (Leslie, 1992) and *SCALA* from *CCP*4 (Winn *et al.*, 2011) (see Table 1). Molecular replacement, model building and refinement were carried out using *Phaser* (McCoy *et al.*, 2005), *Coot* (Emsley & Cowtan, 2004) and *REFMAC* (Murshudov *et al.*, 2011), respectively (see Table 2). The PDB codes for these structures are 3s0y, 3s02, 3s03, 3s06, 3s0h and 3s0w.

2.2. Gel-filtration chromatography and MALLS analysis

A 100 µl sample of MotB-C_{97} at a concentration of 10 mg ml^{-1} was loaded onto a Superdex 200 10/300 gel-filtration column (GE Healthcare) equilibrated with buffer 1 (50 m*M* sodium acetate pH 4.6, 200 m*M* NaCl) or buffer 2 (50 m*M* Bicine pH 9.0, 200 m*M* NaCl) flowing at 0.5 ml min^{-1}. The eluant was passed through an in-line DAWN HELEOS II laser photometer (λ = 658 nm) and an Optilab T-rEX differential refractive-index detector (Wyatt Technologies). A bovine serum albumin (BSA) standard was run in each buffer to normalize the MALLS detectors. Data were analysed in *ASTRA* v.5.3.4.20 (Wyatt), with a value for the refractive-index increment $(dn/dc)_{\rm protein}$ of 0.185 ml g^{-1}. The results are summarized in Table 3.

3. Results

3.1. Overall fold and oligomeric state of *Hp*MotB-C

The structures of MotB-C_{64} and MotB-C_{103} were solved using the crystals of proteolytic degradation products of *Hp*MotB. The MotB-C_{78}, MotB-C_{90} and MotB-C_{97} structures were solved using the crystals of the respective fragments. All variants share the same fold in their common part (represented by MotB-C_{103}), which comprises a five-stranded β-sheet

Table 2
Refinement statistics.

	MotB-C_{64}	MotB-C_{78}	MotB-C_{90}	MotB-C_{97}, low-pH form	MotB-C_{97}, high-pH form	MotB-C_{103}
Resolution range (Å)	20–1.8	30–2.5	30–2.1	30–2.5	30–1.8	30–2.5
R factor†	0.178	0.193	0.181	0.225	0.17	0.181
Free *R* factor‡	0.221	0.253	0.236	0.284	0.21	0.241
Bond-length deviation from ideality (Å)	0.012	0.013	0.014	0.009	0.012	0.015
Bond-angle deviation from ideality (°)	1.3	1.5	1.4	1.2	1.3	1.5
Average *B* (protein atoms) (Å^2)	34	47	29	51	20	24
Average *B* (water molecules) (Å^2)	32	24	32	33	29	26
Copies per asymmetric unit	2	2	4	4	2	2

† $R = \sum_{hkl} \big||F_{obs}| - |F_{calc}|\big| / \sum_{hkl} |F_{obs}|$. ‡ The free *R* factor was calculated using 5% of the data omitted at random.

Table 3
Molecular weights calculated from the static light-scattering results.

Sample	Buffer	pH	Polydispersity through main peak	Molar mass (kDa)
BSA	1	4.6	1.000 (±0.1%)	63.0 ± 0.2
MotB-C_{97}	1	4.6	1.000 (±0.2%)	33.1 ± 0.2
BSA	2	9.0	1.000 (±0.1%)	64.0 ± 0.2
MotB-C_{97}	2	9.0	1.000 (±0.2%)	35.6 ± 0.3

and four α-helices (Fig. 1*a*). The core domain comprising the four-stranded β-sheet β1β4β2β3 and helices α1–α3 is conserved between MotB and Pal (Fig. 1; Roujeinikova, 2008; Parsons *et al.*, 2006). This domain harbours the petal-like loops β2α2 and β3β4 involved in recognition of the carbohydrate moiety of PG (Roujeinikova, 2008) and the strongly conserved residues Asp164, Leu179 and Arg183 (*Hp*MotB numeration) that have previously been implicated in binding of the peptide moiety of PG (Parsons *et al.*, 2006).

*Hp*MotB-C structures reveal a novel dimeric α/β-barrel fold in which the six-stranded β-sheets of the two molecules form a closed β-barrel-like structure stabilized by contacts between helices α2 and α2′ (Fig. 2). The C-terminal helix (α4) of each monomer also participates in dimeric interactions in a domain-swapping manner. The twofold axis in the dimer is orthogonal to the axis of the barrel. This fold differs from that of the superfamily of dimeric α/β-barrel proteins (Reardon & Farber, 1995), in which the β-barrel comprises only eight strands, the twofold axis is approximately parallel to the axis of the barrel and there are no helices at the dimer interface.

To determine the oligomeric solution state, multi-angle laser light scattering (MALLS) analysis coupled to gel-filtration chromatography was carried out on *Hp*MotB-C_{97} at low pH (4.6) and high pH (9.0) using the same buffers as in the crystallization mixture. *Hp*MotB-C_{97} eluted as a single monodisperse peak at both pH values. The derived molecular-weight values (33.1 and 35.6 kDa at pH 4.6 and 9.0, respectively) were consistent with a dimer.

3.2. Structural changes induced by linker unfolding

Crystallographic analysis of the N-terminally truncated *Hp*MotB variants comprising the PG-binding domain and part of the linker revealed that each individual monomer structure in the analysed set adopts one of three conformations representing different intermediate states in the linker-unfolding pathway (Fig. 3). In intermediate I, the petal-like loops β1α1,

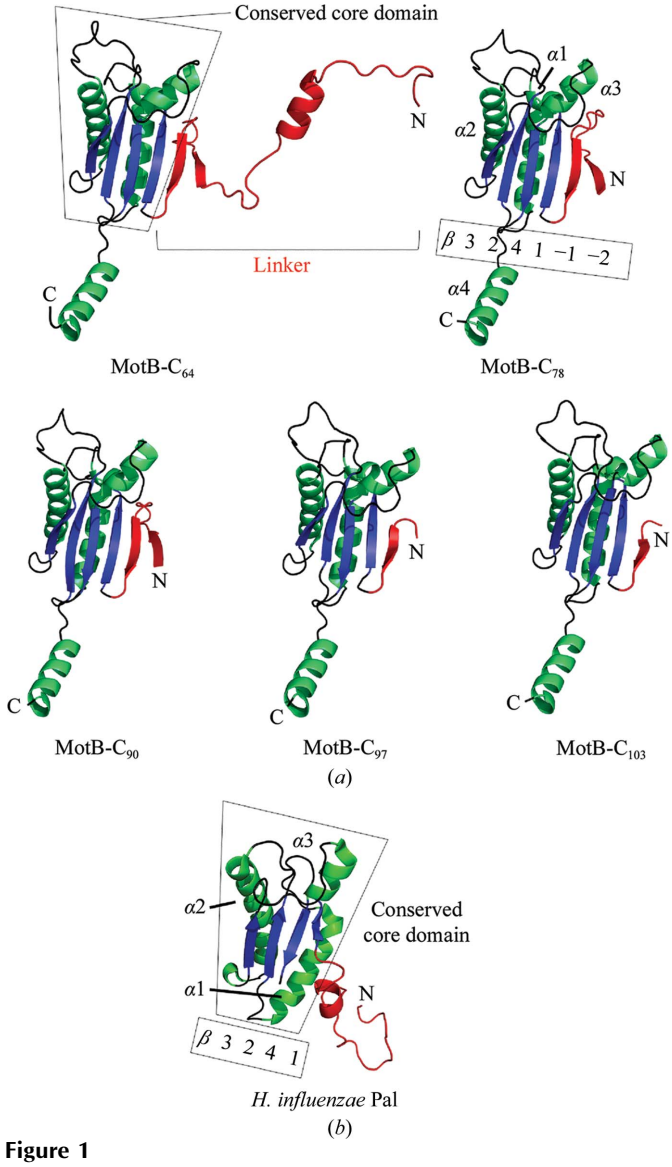

Figure 1
The overall fold of *Hp*MotB-C fragments incorporating part of the linker and comparison with Pal. (*a*) MotB-C_{64}, MotB-C_{78}, MotB-C_{90}, MotB-C_{97} and MotB-C_{103} monomers. The linker (residues 64–112) is coloured red. The β-strand order is indicated. (*b*) Periplasmic domain of *H. influenzae* Pal. The linker (N-terminal 30 residues) is coloured red.

$\beta2\alpha2$ and $\beta3\beta4$ around the PG-binding site completely bury the essential PG-binding residues Leu179 and Arg183 and partially shield Asp164 (Fig. 3*b*). The closed conformation of loop $\beta1\alpha1$ is stabilized by van der Waals contacts between Pro120, Ser121 and Asn122 in $\beta1\alpha1$ and Met222 in $\beta3\beta4$ and by hydrogen bonds between Ser121, Asn127 (main chain) and Ser130 (main chain) in $\beta1\alpha1$ and one of the PG-binding residues, Arg183. Loop $\beta3\beta4$ engages two PG-binding residues, Arg183 and Asp164, *via* hydrogen bonds to Asn225 and to Asn215, Asn225 and Arg221, respectively. The loop residues Ser121, Asn215, Arg221 and Asn225 whose side chains form this hydrogen-bonding network are conservatively substituted by polar residues in the homologous structures of *St*MotB-C_{99} and *Desulfovibrio vulgaris* MotB-C (*Dv*MotB-C; PDB entry 3khn; Fig. 4*a*).

In intermediate II, loop $\beta(-1)\beta(-2)$ of the linker moves away from helix $\alpha1$ concomitantly with the movement of the adjacent loop $\beta3\beta4$. Repositioning of the latter breaks its contacts with loop $\beta1\alpha1$ and disrupts the hydrogen-bonding network with Asp164, resulting in a partially open conformation in which two PG-binding residues, Asp164 and Leu179, become surface-exposed.

In intermediate III strand $\beta(-2)$ dissociates from the β-sheet, while strand $\beta(-1)$ remains the last moiety of the linker still in contact with the core domain. Loops $\beta3\beta4$ and $\beta1\alpha1$ move further away from each other, upon which the third essential PG-recognition residue Arg183 loses hydrogen bonds to Ser121 and Asn225 and becomes surface-exposed.

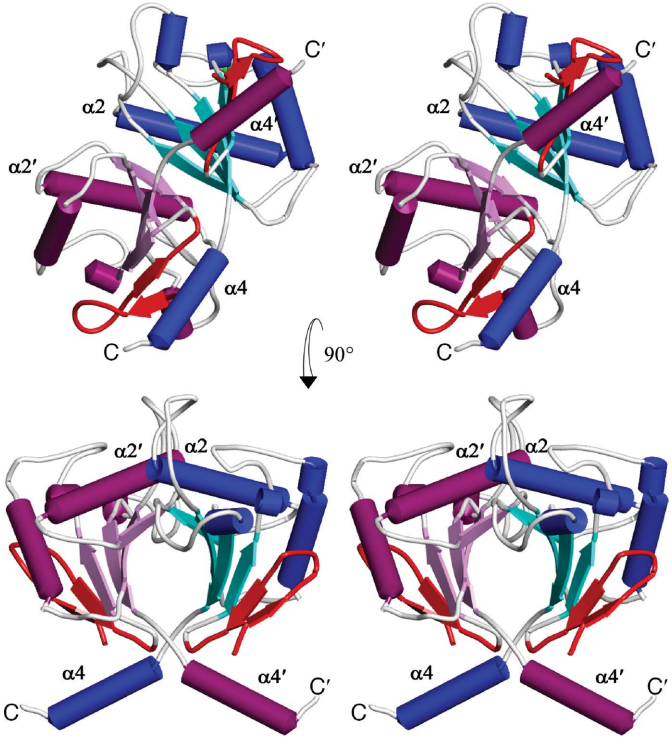

Figure 2
Side and top stereoviews of the MotB-C_{78} dimer. The arrangement of the two subunits was essentially the same for MotB-C_{64}, MotB-C_{78}, MotB-C_{90}, MotB-C_{97} and MotB-C_{103}.

Thus, analysis of the three intermediate states in the linker-unfolding pathway reveals that the conserved PG-recognition residues of MotB are buried when the linker is folded against the conserved core and strongly suggests that linker separation and unfolding is required to fully expose the PG-binding site.

3.3. Comparison to MotB-C from other species

Anchoring of the MotA/MotB complex to PG in a correct orientation is likely to be achieved *via* simultaneous engagement of the two halves of the MotB dimer (Roujeinikova, 2008). Given the conserved nature of PG, we argue that if MotB-C fragments incorporating the linker adopted an active (competent for binding PG) conformation, the juxtaposition of the two PG-binding sites would be similar in fragments from different species. Comparison of the crystal structures of *Hp*MotB-C, *St*MotB-C_{99} and *Dv*MotB-C (Fig. 4*b*) reveals that the dimerization mode in the presence of the linker shows significant species-specific variations, with an $\sim$40° difference in the relative orientation of the two halves of the dimer for each compared pair. Low sequence identity at the dimer interface suggests that interconversion between these forms is unlikely. As a consequence of variation in the angle between the monomers, the juxtaposition of the two PG-binding sites marked by the location of the glycan-binding grooves (Fig. 4*b*) is distinctly different in all three structures. Furthermore, the distance between these grooves in any dimer does not exceed 30 Å. Since the average distance between the adjacent glycan chains in PG is $\sim$50 Å (Meroueh *et al.*, 2006; Koch, 2000), we conclude that neither of the observed forms of MotB-C with the linker folded against the conserved core domain is likely to represent an active (optimal for binding to PG) conformation.

To further understand the structural role of the linker, we compared the dimer of *Hp*MotB-C_{78} with the structure of *Hp*MotB-C_{125}, which has no linker and thus mimics the conformation of MotB-C with an unfolded linker (Fig. 4*b*). This comparison suggested that linker unfolding results in a major reorientation of the two MotB-C subunits and repositioning of the C-terminal helix. Upon this transition, the two glycan-binding grooves become separated by $\sim$50 Å, which may allow association of MotB-C with two sugar chains of PG simultaneously. Such a transition requires disruption of dimeric domain-swapping interactions between the C-terminal helix of one monomer and the folded linker of the second monomer. This suggests that the linker plays an important role in stabilizing the MotB dimer in a configuration that is not competent for binding to PG.

3.4. Implications for the stator activation mechanism

The structural analysis presented here indicates that the folded linker plays a crucial role in suppressing the PG-binding activity of MotB until the stator incorporates into the motor. The conserved residues of *Hp*MotB-C implicated in recognition of the peptide moiety of PG are buried under two petal-like loops $\beta1\alpha1$ and $\beta3\beta4$ when the linker is folded against the conserved core. This result is in line with the

previous observation that these residues are buried under the same two loops in the folded-linker form of *St*MotB-C_{99} (Reboul *et al.*, 2011; Kojima *et al.*, 2009). Upon linker separation, a conserved hydrogen-bonding network that ties the loops to the PG-binding residues becomes broken, exposing them to the solvent. Comparison of the three known homologous MotB-C structures suggests that the linker in its folded form stabilizes the dimer configuration that cannot engage two glycan chains of PG simultaneously. Comparison with the previously reported different configuration that has geometry

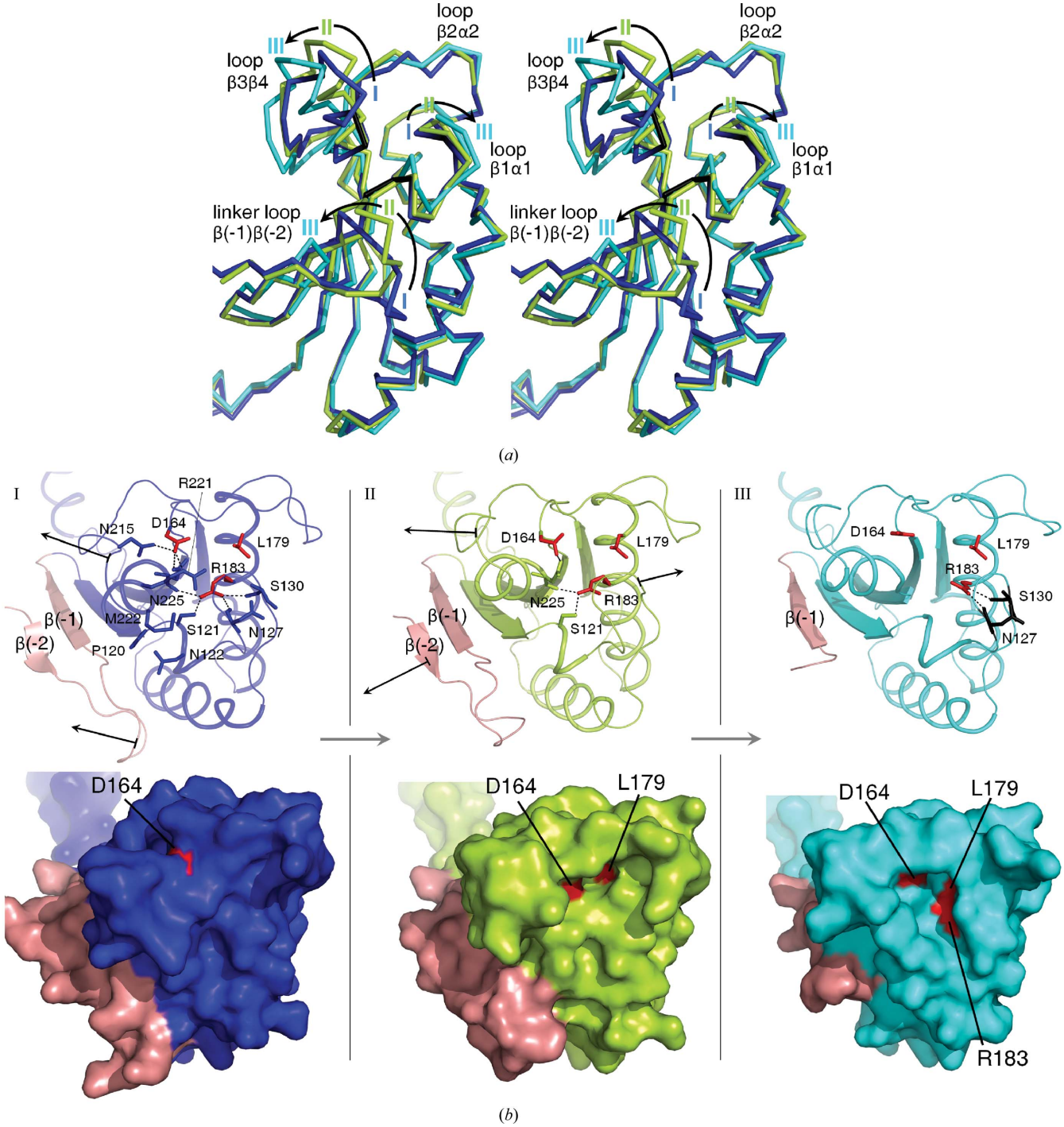

Figure 3
Structural changes induced by linker unfolding. (*a*) Stereoview of the superposition of the structures of three different intermediate states in the linker-unfolding pathway: intermediate I (blue; exemplified by MotB-C_{64}, chain *A*), intermediate II (green; exemplified by MotB-C_{78}, chain *B*) and intermediate III (turquoise; exemplified by MotB-C_{97}, high-pH form, chain *B*). Structures of MotB-C_{64} (chain *A*), MotB-C_{78} (chain *A*) and MotB-C_{90} were trapped in the crystal in intermediate state I, MotB-C_{97} (high-pH form, chain *B*) and MotB-C_{103} in state III and the remaining structures in state II. (*b*) Disruption of stabilizing interactions between PG-binding residues Asp164, Leu179 and Arg183 and petal-like loops $\beta1\alpha1$ and $\beta3\beta4$ upon transition from state I to II and III (top) and the resultant increase in the surface accessibility of the former (bottom). Arrows indicate the directions of movement of loops $\beta(-1)\beta(-2)$, $\beta1\alpha1$ and $\beta3\beta4$ upon linker detachment.

optimal for PG binding suggests that linker unwinding and a major reorientation of the two halves of the MotB-C dimer is required for MotB insertion into the PG mesh. Thus, our analysis reveals a novel dual mechanism of inhibition of PG-binding activity of stator precomplexes by the folded MotB linker.

Our structural analysis is consistent with the results of previous genetics and biochemical experiments that pointed

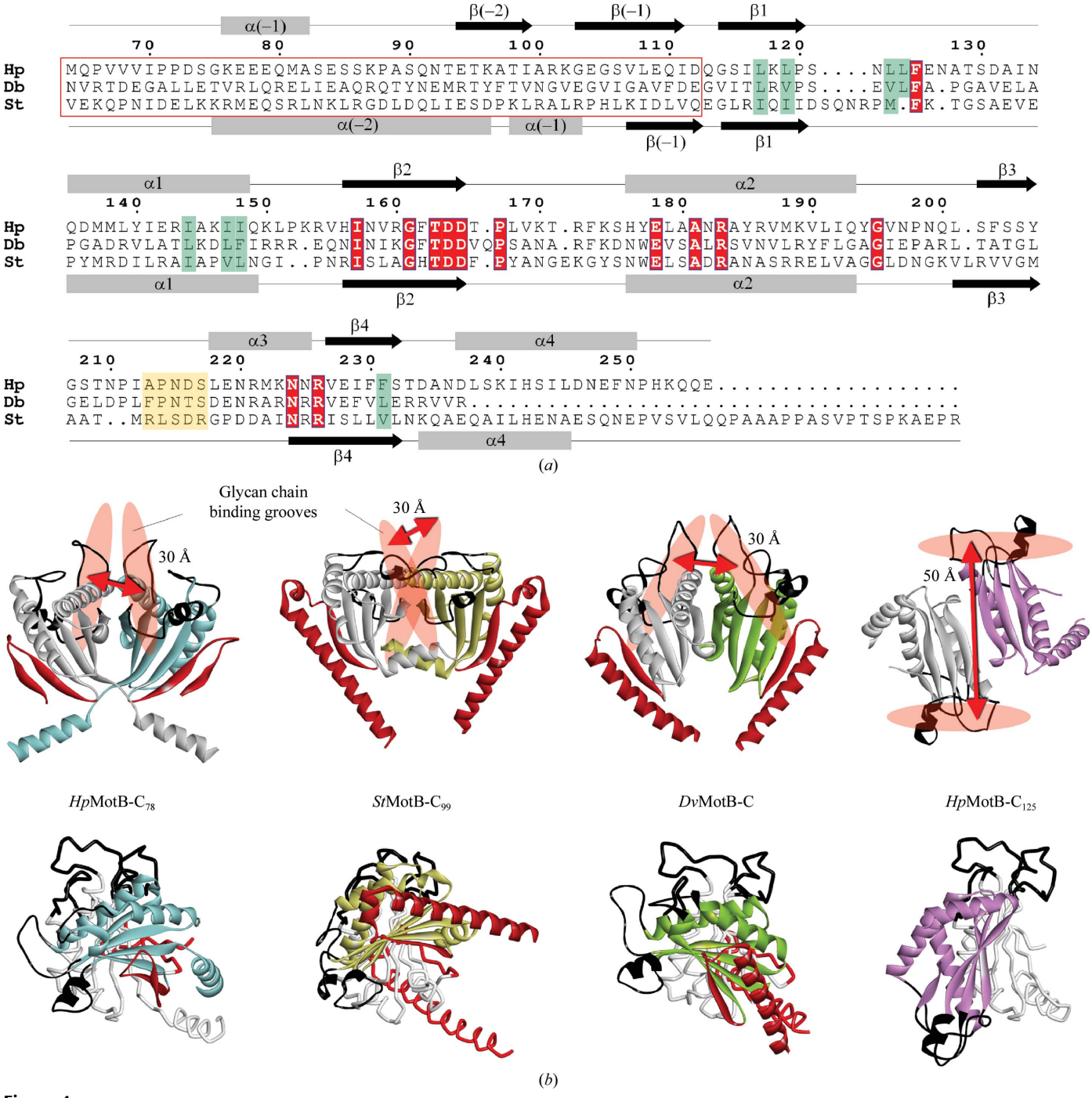

Figure 4
Comparison to MotB-C from other species. (*a*) Structure-based sequence alignment of the periplasmic regions of *Hp*MotB, *St*MotB and *Dv*MotB. The secondary structures of *Hp*MotB-C_{64} and *St*MotB-C_{99} are shown above and below the alignment, respectively. Linker residues are indicated by the red frame. Conserved residues are shown in white on a red background. FlgI cross-linking residues and hydrophobic residues that form a surface-exposed patch upon linker detachment are highlighted in orange and green, respectively. (*b*) Comparison of the *Hp*MotB-C_{78}, *St*MotB-C_{99}, *Dv*MotB-C and *Hp*MotB-C_{125} dimers. The linker and petal-like loops $\beta1\alpha1$, $\beta2\alpha2$ and $\beta3\beta4$ around the peptidoglycan-binding site are coloured red and black, respectively. The top view highlights the differences in the juxtaposition of the two putative glycan chain-binding grooves. The location of the groove was established by superimposing the respective coordinates with the previously reported model of the *Hp*MotB-C_{125} complex with the sugar chain of PG (Roujeinikova, 2008). The bottom view highlights the variations in the relative orientation of the two halves of the MotB-C dimer. This view was generated by overlapping all dimers over one half, which is shown at the back in black-and-white tube representation.

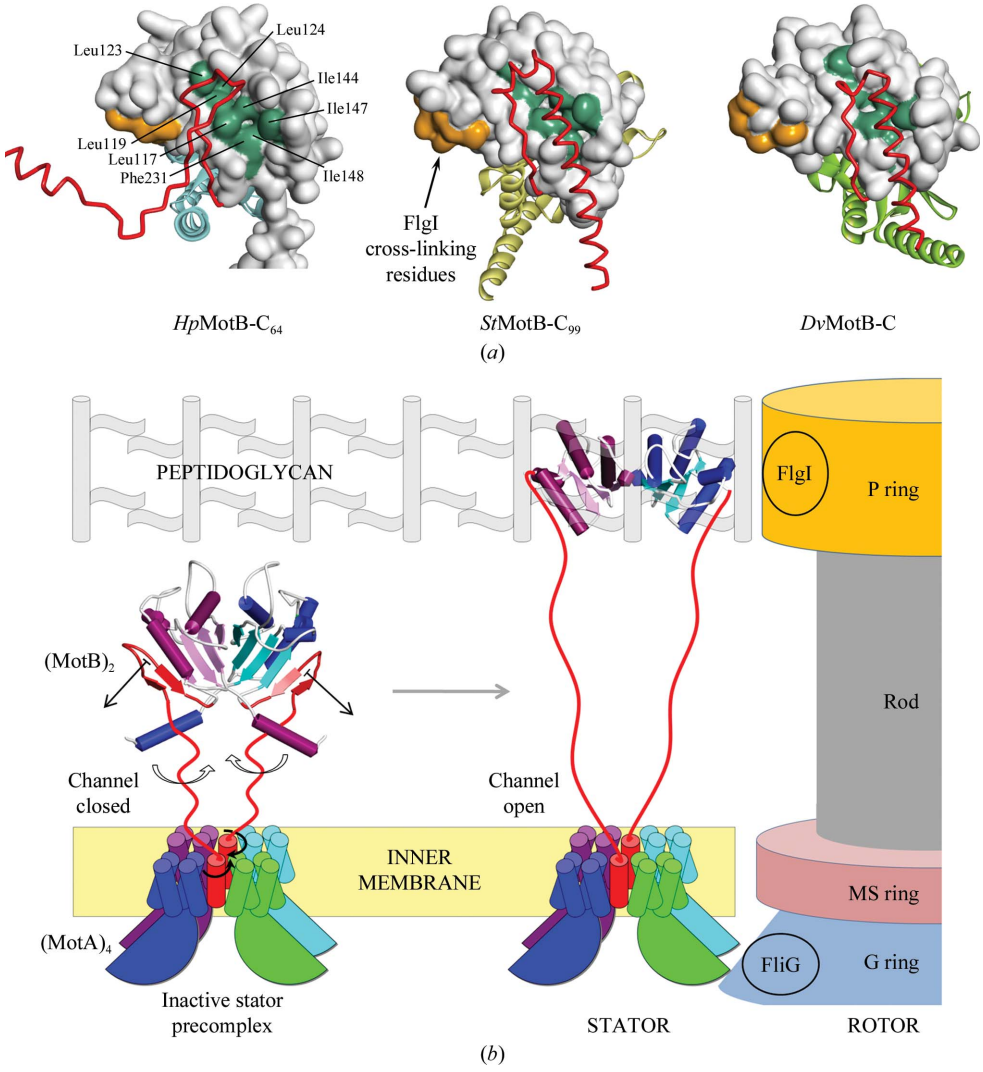

Figure 5
Structural basis for stator assembly and activation. (*a*) Strongly conserved hydrophobic residues (green) exposed upon linker detachment and unfolding. FlgI cross-linking residues are shown in orange. The linker is coloured red. (*b*) Proposed molecular mechanism of $MotA_4MotB_2$ incorporation into the motor and activation.

towards the linker region being mechanistically important for MotB function. No binding was detected between PG and the functional *E. coli* MotB variant in which the PG-binding domain was replaced by the PG-binding domain of Pal (Hizukuri *et al.*, 2009), suggesting that the TM helix and the linker play a role in suppressing the PG-binding activity. It appears that the distance restraint imposed by the membrane-anchored folded linker (Kojima *et al.*, 2009) is not the only factor inhibiting binding to PG. When such a restraint was eliminated by removing the TM anchor, the resultant MotB fragment comprising the linker and PG-binding domain could not be co-isolated with PG (Kojima *et al.*, 2008). Our structural analysis reveals the structural basis of inhibition of PG-binding activity by the linker in fragments lacking the TM helix and thus provides an explanation of this phenomenon.

It has been proposed that the periplasmic P ring of the motor, which is composed of multiple copies of the protein FlgI, may provide binding sites for stator assembly and that linker unfolding may be triggered by interaction between MotB-C and FlgI (Hizukuri *et al.*, 2010). Cross-linking experiments demonstrated *in vivo* proximity between *St*MotB residues 246–250 and FlgI, but the entire MotB–FlgI interface is unknown. Importantly, our structural analysis predicts that linker separation from the MotB conserved core domain would expose a surface patch of strongly conserved hydrophobic residues (Leu117, Leu119, Leu123, Leu124, Ile144, Ile147, Ile148 and Phe231 in *Hp*MotB) in the vicinity of the FlgI cross-linking residues (Fig. 5*a*). This points to the possible location of the second part of the FlgI docking site.

The requirement for a major reorientation of the two halves of the MotB-C dimer prior to insertion into the PG mesh next to the motor has a prominent implication for the mechanism of stator activation. We speculate that the rotation of the two C-terminal domains of MotB twists the linker and this in turn causes rotational displacement of its two TM helices (Fig. 5*b*). By using an analogy with a potassium channel, Schmitt (2003) previously postulated that rotational displacement of MotB TM helices opens the permeation pathway for protons. Combined, the analysis presented here indicates that the MotB linker region plays a pivotal role in the mechanism of stator assembly and activation. Our data are consistent with a model that involves the following conformational transitions in MotB (Fig. 3*b*): (i) linker separation and unfolding, triggered by contact with the rotor; (ii) exposure of the conserved PG-binding residues; (ii) alignment of the two PG-binding sites *via* reorientation of the two conserved core domains and insertion into the PG mesh; and (iv) opening of the proton channel *via* rotational displacement of the two MotB TM helices.

This work was supported by the Australian Research Council (ARC DP1094619 to AR). AR is an ARC Research Fellow.

References

Emsley, P. & Cowtan, K. (2004). *Acta Cryst.* D**60**, 2126–2132.

Hizukuri, Y., Kojima, S. & Homma, M. (2010). *J. Biochem.* **148**, 309–318.

Hizukuri, Y., Morton, J. F., Yakushi, T., Kojima, S. & Homma, M. (2009). *J. Biochem.* **146**, 219–229.

Hosking, E. R., Vogt, C., Bakker, E. P. & Manson, M. D. (2006). *J. Mol. Biol.* **364**, 921–937.

Koch, A. L. (2000). *Arch. Microbiol.* **174**, 429–439.

Kojima, S., Furukawa, Y., Matsunami, H., Minamino, T. & Namba, K. (2008). *J. Bacteriol.* **190**, 3314–3322.

Kojima, S., Imada, K., Sakuma, M., Sudo, Y., Kojima, C., Minamino, T., Homma, M. & Namba, K. (2009). *Mol. Microbiol.* **73**, 710–718.

Leake, M. C., Chandler, J. H., Wadhams, G. H., Bai, F., Berry, R. M. & Armitage, J. P. (2006). *Nature (London)*, **443**, 355–358.

Leslie, A. G. W. (1992). *Jnt CCP4/ESF–EACBM Newsl. Protein Crystallogr.* **26**.

McCoy, A. J., Grosse-Kunstleve, R. W., Storoni, L. C. & Read, R. J. (2005). *Acta Cryst.* D**61**, 458–464.

Meroueh, S. O., Bencze, K. Z., Hesek, D., Lee, M., Fisher, J. F., Stemmler, T. L. & Mobashery, S. (2006). *Proc. Natl Acad. Sci. USA*, **103**, 4404–4409.

Murshudov, G. N., Skubák, P., Lebedev, A. A., Pannu, N. S., Steiner, R. A., Nicholls, R. A., Winn, M. D., Long, F. & Vagin, A. A. (2011). *Acta Cryst.* D**67**, 355–367.

O'Neill, J. & Roujeinikova, A. (2008). *Acta Cryst.* F**64**, 561–563.

Parsons, L. M., Lin, F. & Orban, J. (2006). *Biochemistry*, **45**, 2122–2128.

Reardon, D. & Farber, G. K. (1995). *FASEB J.* **9**, 497–503.

Reboul, C. F., Andrews, D. A., Nahar, M. F., Buckle, A. M. & Roujeinikova, A. (2011). *PLoS One*, **6**, e18981.

Roujeinikova, A. (2008). *Proc. Natl Acad. Sci. USA*, **105**, 10348–10353.

Schmitt, R. (2003). *Biophys. J.* **85**, 843–852.

Terashima, H., Kojima, S. & Homma, M. (2008). *Int. Rev. Cell. Mol. Biol.* **270**, 39–85.

Wilson, M. L. & Macnab, R. M. (1988). *J. Bacteriol.* **170**, 588–597.

Winn, M. D. *et al.* (2011). *Acta Cryst.* D**67**, 235–242.